Analysis of Turbulent Underexpanded Jets, Part II: Shock Noise Features Using SCIPVIS

J.M. Seiner*
NASA Langley Research Center, Hampton, Virginia
and
S.M. Dash† and D.E. Wolf‡
Science Application Inc., Princeton, New Jersey

SCIPVIS, the computational model discussed in Part I of this paper, is assessed in predicting the complicated flow structure associated with shock-containing plumes. In addition, the analysis in this study examines this code's applicability as a basic part of a program for estimating broadband shock noise radiation. The results of this study show that excellent agreement exists between predicted and measured static pressure distributions for both underexpanded and overexpanded flow cases considered. Of the three turbulence closure models incorporated in the SCIPVIS code, the kW model of Spalding produces the most uniform agreement with measurement. The $k\epsilon 2$ model of Launder consistently overestimates plume spreading for supersonic jets with exit Mach numbers in the range $1<M_e<2$. Dash's $k\epsilon 2$-cc compressibility corrected version of Launder's model underestimates plume spreading. Good qualitative agreement was also obtained between the measured longitudinal turbulence intensity and that predicted by the code for the same trial case. Comparison of measured and predicted broadband shock noise spectrum peak values were found to be in excellent agreement. This utilized a variant of the Harper-Bourne and Fisher phase-array model: the effective shock spacing was reinterpreted as the value at the end of the plume potential core, determined herein by the SCIPVIS code.

Introduction

THE major failure for any widespread application to jet aircraft noise of the theoretical shock noise models of either Lighthill[1] or Ribner[2] has been the consistent lack of any detailed knowledge of the supersonic jet plume's evolving turbulent mixing layer and decaying shock structure. Over the last several years, however, significant progress has been made in the identification of acoustic properties associated with aerodynamic features of these shock containing supersonic flows.[3-8] These efforts have focused primarily on the broadband shock noise component, which has been found to be the dominant acoustic component for engine-type flows in an aircraft's forward arc. These experimental studies indicated that the downstream shock structure (i.e., those shocks located near the end of the initial mixing region) was strongly dependent on the development of the turbulent mixing layer, and that this dependence exerts a strong influence on both amplitude and peak frequency of broadband and shock noise. The existence of strong shocks in the jet plume, such as occurs with the formation of a large Mach disk, was also found to significantly reduce the amplitude of shock noise due to a corresponding decrease in the strength of the downstream shock structure which occurs due to nonisentropic losses produced by the strong shocks. To implement these experimental discoveries into existing shock noise theories required at a minimum a realistic prediction of the decaying shock structure in a supersonic jet.

In Part I[16] of this article, a new numerical plume prediction model, SCIPVIS, is described which accounts for the interactive coupling of wave and turbulent mixing processes, and accounts for the influence of compressibility on turbulent shear flows. The objective of this paper is to evaluate the capabilities of this new code regarding its ability to predict the evolving plume shock and turbulence structure. Specifically, this code shall be exercised over a similar range of nozzle exit conditions as previously obtained through experimental observations.[4-7] Thus, comparisons between measured and computed results will be made for both under- and overexpanded flows for several supersonic exit Mach numbers including the sonic nozzle.

The comparisons made in this paper generally take the form of relating the predicted and measured static pressure distributions in the evolving jet plume. After these comparisons are made, this paper shows, for a specific case, how well this new code can predict the spectrum peak value for broadband shock noise, and illustrates the effect of flight Mach number on this peak value. The theoretical shock noise models of Lighthill[1] and Ribner[2] employ shock interaction integrals that require detailed information concerning shock strength and position for all shock interfaces penetrating the turbulent mixing layer, and, in addition, require knowledge of the turbulent stress tensor just upstream of the shock interface. Thus, as a final comparison, this paper shows the agreement obtained between the measured longitudinal turbulent component and that derived from the numerical code for the typical underexpanded shock-containing turbulent mixing layer.

Description of General Plume Features

As a aid to defining general regions in a shock-containing supersonic jet plume that are relevant to the remainder of this paper, Fig. 1 illustrates, as an example, the underexpanded flow produced by a supersonic nozzle with a nominal exit Mach number of 2, operating with an exit pressure ratio of $P_e/P_a = 1.47$. To improve clarity in shock wave details the radial axis is magnified by a factor 2.5 times that used for the axial direction so that as a result angles of shocks and spread rates are not shown in true perspective.

Presented as Paper 83-0705 at the AIAA 8th Aeroacoustics Conference, Atlanta, Ga., April 11-13, 1983; received April 28, 1983; revision received May 7 1984. This paper is declared a work of the U.S. Government and therefore is in the public domain.

*Research Engineer, Aerocoustics Branch, ANRD. Member AIAA.
†Technical Director, Propulsion Gas Dynamics Division. Member AIAA.
‡Research Scientist, Propulsion Gas Dynamics Division. Member AIAA.

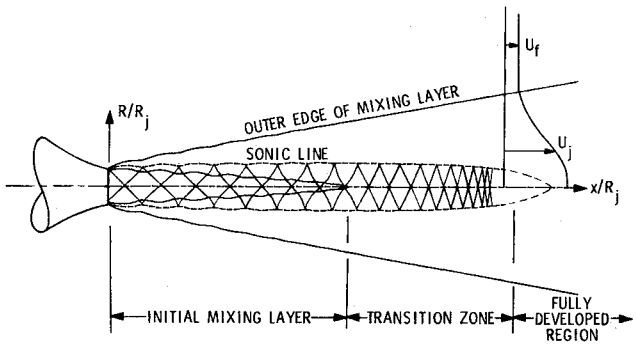

Fig. 1 General plume features.

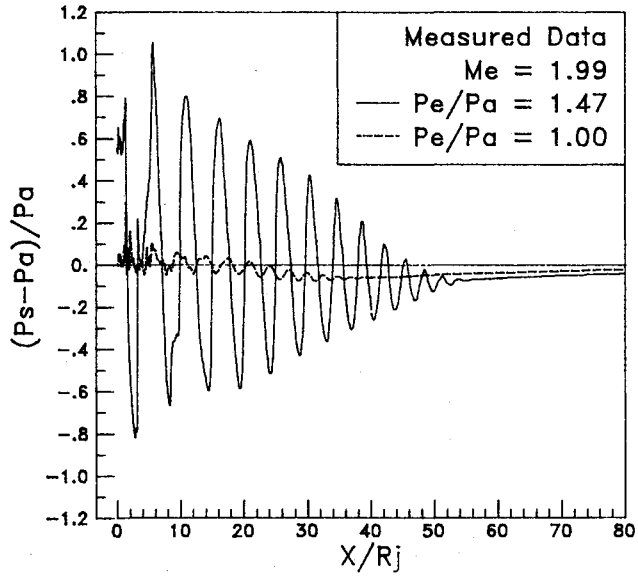

Fig. 2 Typical measured centerline static pressure decay showing entrainment effect.

The inner edge of the mixing layer is outlined by the interior cone whose axial extent defines the length of the initial mixing layer. For this example this occurs at $x \simeq 38R_j$. Inside this region shock noise generation is not considered important as long as the jet plume is composed only of a weak wave system as in Fig. 1. With strong shocks (i.e., Mach disks), pockets of high turbulence intensity can be observed even along the jet centerline in this initial region due to fluid rotation induced by the strong shocks (see Ref. 16 or Ref. 9 for details). The outer solid lines in Fig. 1 show the radial extent of the outer edge of the mixing layer which, along with the lower edge of the mixing layer, characterizes the rate of plume spreading. The region of supersonic flow is enveloped by the sonic line, shown here by the dashed cone. It represents the boundary for shock wave terminations, and indicates that the region for supersonic flow extends to $x \simeq 70R_j$ in this example.

The shocks illustrated in Fig. 1 are shown terminating at the sonic line at the actual scaled locations predicted by the code, which, for this case, will be later shown to be in good agreement with measurements. It is evident that the repetitive shock wave pattern, which forms the familiar diamond-shape cell in schlieren photographs, extends well beyond the nozzle exit, providing a large area for shock-turbulence interaction. Those shocks located near the end and beyond the initial mixing region are referred to herein as the downstream shocks. All shocks in the turbulent mixing zone are curved since they propagate into a region of nonuniform mean flow. This curvature, along with the radial increase in sonic line location, is responsible for the gradual steepening of the wave angle

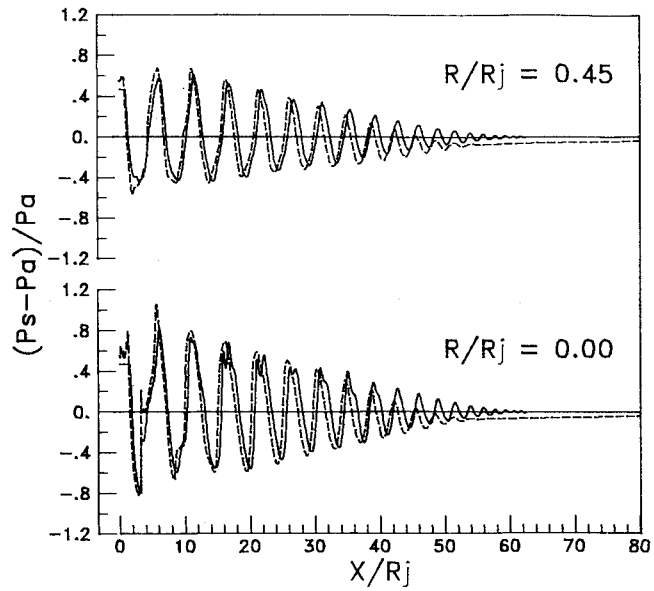

Fig. 3 Comparison of predicted and measured static plume pressure for underexpanded $M_e = 1.99$, $P_e/P_a = 1.47$ flow;——predicted *(kW)* $M_f = 0.15$,----measured.

relative to the mean flow. This leads to the observable decrease in shock cell spacing with axial distance. Eventually a point is reached, in this example at $x \simeq 61R_j$, where the shock can properly adjust the flow and the wave is cancelled. This occurs before the end of the supersonic core.

Comparison of Measured and Calculated Plume Static Pressure

In this section results obtained using the SCIPVIS code are compared to new and previous experimental static pressure measurements for three nozzle exit Mach numbers of 1.00, 1.41, and 1.99. The method used to acquire these data has been described previously in Refs. 4 and 5.

All of the three two-equation turbulence closure models incorporated in the code (see Part I) are investigated in this study. The performance of the SCIPVIS code using all three turbulence closure models for one particular case where corresponding experimental data existed (i.e., $M_e = 1.99$, $P_e/P_a = 1.47$) is discussed in Part I, as is the performance for a balanced pressure Mach 2.2 jet exhausting into still air. The compressibility modified kW model discussed in Part I provided the best match to experimental observations. Thus, in the present investigation, only the kW option is exercised for the $M_e = 1.99$ nozzle; however, all three models are utilized for comparison to the $M_e = 1.00$ and 1.41 nozzles to determine if the kW option can continue to provide the better match to experiments over an extended range of exit Mach number conditions.

All computations reported in this study using the SCIPVIS code were performed on the NASA Langley Jet Noise Laboratory PDP 11-34 computer, where the code proceeded at a rate of approximately 0.9 jet radii per minute using 41 radial grid points. The supersonic nozzle exit Mach numbers, M_e, were previously determined from nozzle exit calibrations, and, therefore, are not nominal values. All computational cases were run using a total temperature of 289.3 K, which represents a reasonable average for all experimental cases.

Mach 1.99 Static Pressure Comparisons

In this section, comparisons of measured and calculated plume data are carried out for both typical under- and overexpanded flows for a $M_e = 1.99$ supersonic nozzle containing a weak wave system. The effect of the entrainment-induced ex-

ternal stream velocity on the predicted plume behavior is also examined to determine if the predicted plume structure asymptotes properly to the static flight experimental conditions.

In Fig. 2 the measured centerline static pressure illustrates the decaying shock structure that occurs with plume spreading rates for the mildly underexpanded condition of $P_e/P_a = 1.47$. This condition matches the illustrated plume flowfield of Fig. 1. From these data it is evident that the shock wave strength rapidly decays with distance from the nozzle exit. The data in Fig. 2 are shown normalized by the surrounding atmospheric pressure P_a. Recalling Fig. 1, the minimum pressure peaks in Fig. 2 correspond to the axial locations for shock reflection along the jet centerline, and the pressure maxima correpond to the end of a compression zone which is approximately the axial location where shocks terminate at the sonic line.

Also shown in Fig. 2 is the centerline static pressure distribution for the $M_e = 1.99$ nozzle for what is commonly referred to as perfectly expanded flow (i.e., $P_e/P_a = 1.0$). This condition is shown to illustrate a regular feature of all jet-like flows. As part of the entrainment process, the static pressure falls below atmospheric pressure just after the initial mixing region ($x \simeq 22R_j$ for fully expanded flow), and continues to do so through the transition region. In the fully developed region of the flow the static pressure begins to asymptote to normal atmospheric pressure, only reaching it when the axial mean flow is completely dissipated. This process is also evident in the underexpanded case in Fig. 2, when after its initial mixing region ($x \simeq 38R_j$), the average static pressure falls below atmospheric. Near the end of the transition zone the shocks disappear and there is a general recovery of the centerline static pressure similar to what is observed for the fully expanded jet.

Since SCIPVIS does not as yet contain the necessary potential flow iterative coupling required to accurately predict jet entrainment-induced effects, the calculated static pressure distributions shown in this study will fall symmetrically about the atmospheric pressure line. This presents no real difficulty, except for better appearing comparisons, since the shock wave static pressure decay is the more important parameter in this study.

Figure 3 shows the general agreement obtained between the measured static pressure and that predicted by SCIPVIS using the kW turbulence model option and a flight Mach number estimate of $M_f = 0.15$. Figure 3 demonstrates that SCIPVIS represents a remarkable improvement over what was previously obtained in Ref. 5 using an inviscid Euler code. Both the amplitude and shock spacing of the measured data are well represented by prediction. The deviation between measured and predicted average pressure in the transition zone due to entrainment-induced effects can be noted as discussed previously. In the near-field region of plume development, however, the variation of the sonic line and its shock termination locations are predicted very well by SCIPVIS as shown by Fig. 4. This indicates that the evolution of the plume's turbulent mixing layer for the initial region has been modeled with adquate precision.

Figure 5 shows the remarkably good agreement obtained in this case for the predicted centerline Mach number distribution and that determined from total and static tube pressure measurements. The fully expanded case is included to show that the underexpanded jet behaves in a similar fashion but with initial mixing and fully developed regions occurring further downstream. Figure 5 also shows that the predicted flow's fully developed region occurs slightly downstream of that observed from measurement. At this point then, it is worthwhile to determine the sensitivity of the predicted results with the selection of the code's forward flight Mach number parameter M_f.

Considering again the trial case of Fig. 3, Fig. 6 shows the predicted centerline static pressure distribution obtained using freestream Mach numbers of $M_f = 0.15$ and 0.75. From this comparison it is evident that the decay rate of downstream shocks is greatly reduced, and that there is a marked increase in shock spacing with increasing flight Mach number. Figure 7 shows how the predicted increase in shock cell spacing at the end of the potential core L_e depends on flight Mach number. Here the measured shock cell spacing L_e for this trial case is used as a normalizing parameter. The predicted value for L_e extrapolated from the predicted flight results in Fig. 7 agrees closely with the measured value for L_e. The slope of the best fit line is 0.28. For purposes of the static pressure comparisons in the remainder of this paper, a value of $M_f = 0.15$ is selected. Appropriate simulation of the static jet plume ($M_f = 0$) will be better modeled with the future incorporation of a potential flow solution for the outer regions of the flow which should eventually permit using the actual entrainment-induced external stream velocity variation which is now taken to be an assumed constant value.

A typical example of the SCIPVIS code's predictive capability of overexpanded flow is shown in Fig. 7 for the $M_e = 1.99$ nozzle with $P_e/P_a = 0.749$. Figure 8 shows the agreement obtained along the jet centerline and along the line

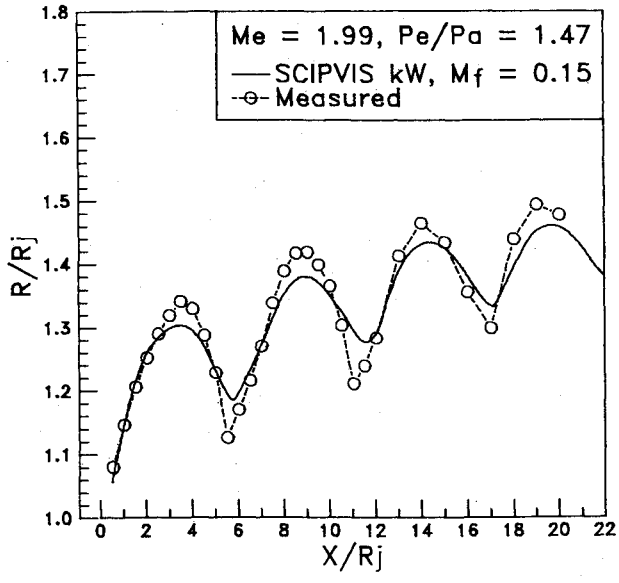

Fig. 4 Variation of predicted and measured sonic line for underexpanded $M_e = 1.99$, $P_e/P_a = 1.47$ flow.

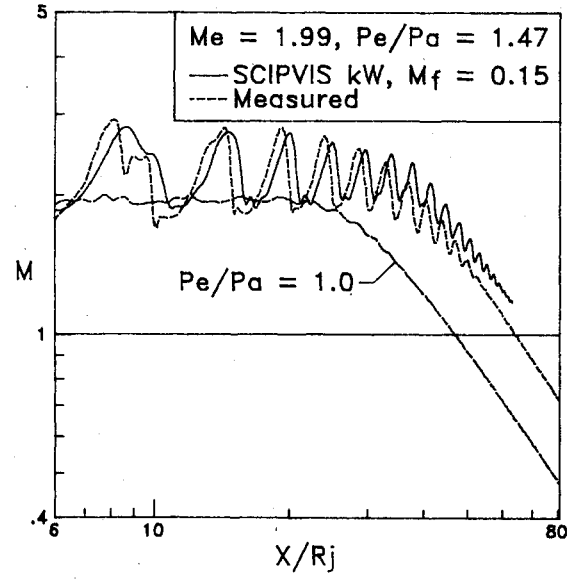

Fig. 5 Comparison of predicted and measured centerline Mach numbers.

$r=0.75R_j$. The centerline distribution represents the axial extent of available data for this case, and, as is evident, the code predicts the irregular-looking pressure data with remarkable precision. The off-axis data show that there is a good correspondence obtained for the location of the first three shock cells; however, the amplitude for the first pressure maxima differs considerably between measured and predicted results. It is known that the oblique shock strength is a strong function of radial position as the sonic line is approached, so that small differences in plume spreading could account for this discrepancy in the amplitudes of the pressure maxima. Figure 8 also indicates that there is a marked difference in the shock spacing of the downstream shock structure, again suggesting that the measured jet plume has a faster plume spreading rate.

We now consider the predictive capabilities of the SCIPVIS code for the other two exit Mach number cases, and examine the outcome for all three turbulence closure models.

Mach 1.41 Static Pressure Plume Comparisons

For this exit Mach number only one trial case is considered; the mildly underexpanded flow where $P_e/P_a=1.36$. For these comparisons a "flight" Mach number of 0.15 are selected as being representative of the entrainment-induced external stream velocity for static conditions. The experimental data are shifted downstream $0.233R_j$ to correspond to a position where the static ports are located on the probe body. With lower Mach number flows the static probe provides a more realistic account of stream Mach number when used in conjunction with a supersonic total pressure tube. This was not required for the $M_e=1.99$ condition, since the static probe is designed for this elevated Mach number.

Figures 9a and 9b, respectively, show the comparison between the measured and predicted static plume pressure for the $k\epsilon 2$, $k\epsilon 2$-cc, and kW turbulence closure models. Figure 9a displays the centerline results, which represent the axial extent of measured data; Fig. 9b displays the results along the radial line $R=0.9R_j$. Is it quite evident from all centerline comparisons for this case that the near-field predominantly inviscid wave structure is not significantly influenced by the turbulence (see discussion in Ref. 9). The off-axis data, which extend to $x/R_j\simeq 30$, clearly show that the $k\epsilon 2$-cc model overpredicts and the $k\epsilon 2$ model underpredicts the shock cell spacing of the downstream shocks. As found in Part I of this article, the kW model appears to provide the best match to experimental observations. The influence of jet-induced entrainment effects on the overall solution[9] remains to be resolved and should improve overall agreement with experimental data.

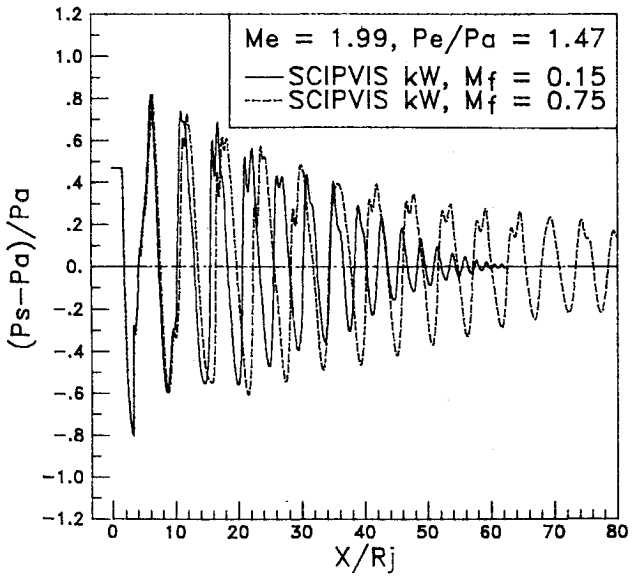

Fig. 6 Effect of flight Mach number on predicted static plume pressure.

Mach 1.00 Static Plume Pressure Comparisons

Similar to what was done in the $M_e=1.41$ case, the experimental data have been shifted in these comparisons $0.241R_j$ downstream to correspond to the locations of the probe's static ports (the sonic nozzle has a smaller exit diameter). The SCIPVIS code was run with the selection of an exit Mach number of 1.02, a total temperature of 340 K, and a flight Mach number of $M_f=0.25$. The computational results shown in this section were made for the underexpanded condition $P_e/P_a=1.62$, which matches previously acquired experimental data for the sonic nozzle.

Figures 10a and 10b, respectively, demonstrate the agreement obtained between measured and predicted static plume pressure for the $k\epsilon 2$ and $k\epsilon 2$-cc turbulence closure models. Figure 10a displays the centerline data, and Fig. 10b displays the off-axis measurements and predictions. The measurements in the off-axis data refer to the radial location $r=0.9R_j$, and the predictions refer to the radial location $r=0.75R_j$. By virtue

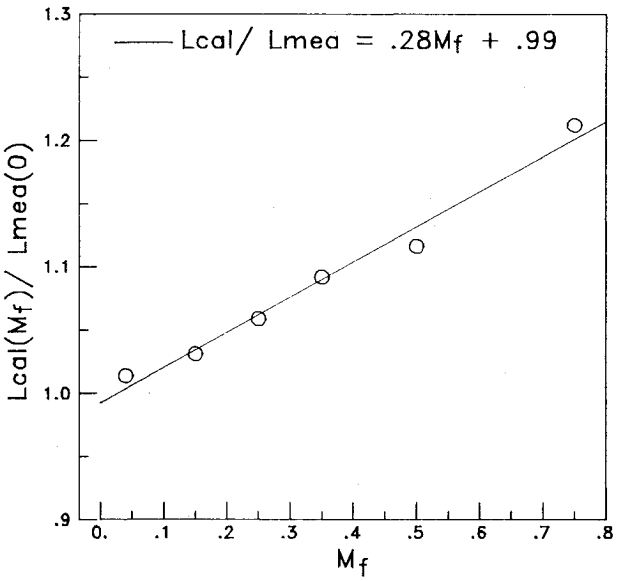

Fig. 7 Effect of flight Mach number on predicted (kW) shock cell spacing at end of potential core relative to measured static condition.

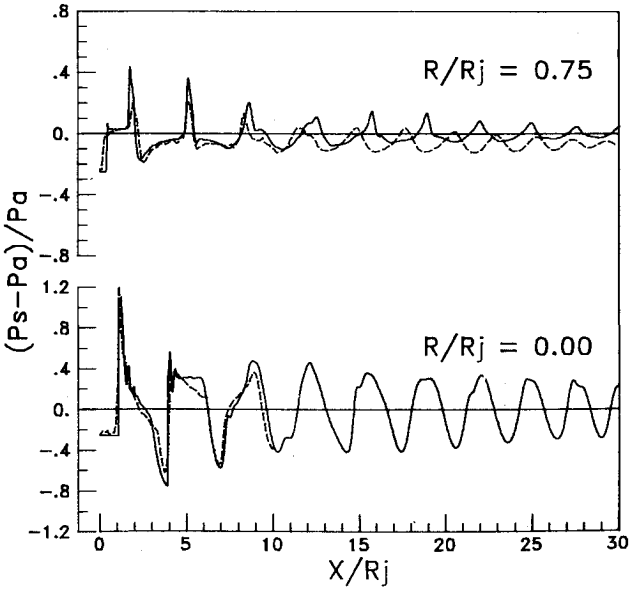

Fig. 8 Comparison of predicted (kW, $M_f=0.15$) and measured static plume pressures for overexpanded $M_e=1.99$, $P_e/P_a=0.749$ flow.

of the agreement between the first few pressure maxima, this difference in radial location suggests that there is a significant difference between the measured and predicted plume structures. Also unusual is the very rapid decay of the measured static pressure distribution along the centerline after the fifth shock cell. Subsequent experimental investigations indicated that this enhanced decay rate was accompanied by the onset of jet screech. These investigations demonstrated that reduction of the screech amplitude reduced the enhanced decay rate significantly.

The effects of compressibility are small near sonic conditions, as evidenced by the close agreement between the $k\epsilon 2$ and $k\epsilon 2$-cc turbulence models. As exhibited in Fig. 2 of Part I of this article, the $k\epsilon 2$-cc model reduces to the $k\epsilon 2$ model as compressibility diminishes. The kW model would underestimate the mixing in lower Mach number situations such as this since its coefficients are fixed.

When considering the overall capability of the SCIPVIS code to predict measured shock structures for the range of conditions presented in this study, it is clear that SCIPVIS represents a significant advance to the area of computational fluid dynamics. Before this code, the first author, at least, could not readily assess the validity of the experimental data. The overall agreement obtained thus far presents a real incentive to make further improvements to this code, particularly in the area of including the entrainment-induced velocity effects and even perhaps to include plume resonance effects as exhibited by the sonic nozzle data. Using the present version of this code, those features required to eventually develop this code into a broadband shock noise prediction routine will be examined next.

Broadband Shock Noise and the SCIPVIS Code

In this section, those fundamental elements required to eventually develop the SCIPVIS code into an effective tool for prediction of broadband shock noise will be considered. In its most elemental form a good noise prediction model must be capable of predicting the peak frequency, spectral shape, amplitude, and directivity for sound radiated by the fluid sources. In the case of broadband shock noise, the model must make a realistic estimate of the shock strength, shock spacing, and turbulence structure over an extensive region of the plume development. While all three of these items are essentially interactive, each item will be discussed individually in the following subsections.

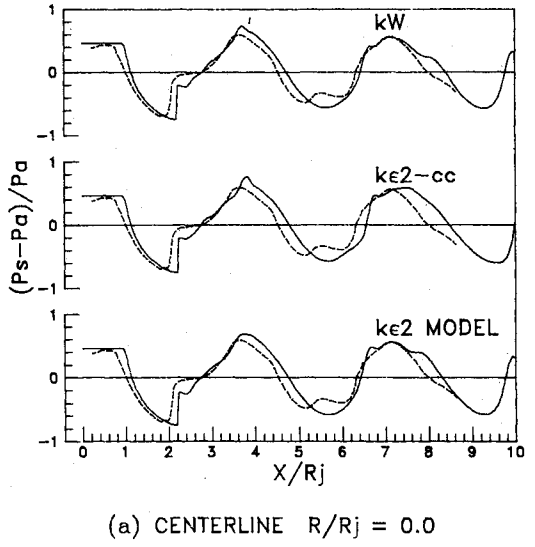

(a) CENTERLINE R/Rj = 0.0

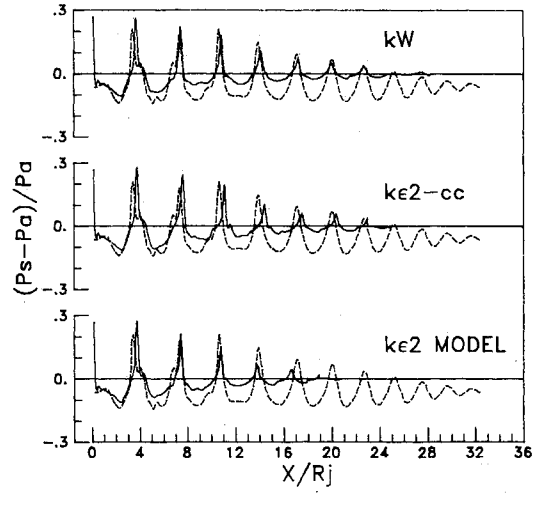

(b) OFF−AXIS R/Rj = 0.9

Fig. 9 Effect of turbulence closure model on predicted plume static pressure for underexpanded $M_e = 1.41$, $P_e/P_a = 1.36$ flow;—— predicted $M_f = 0.15$; ----measured.

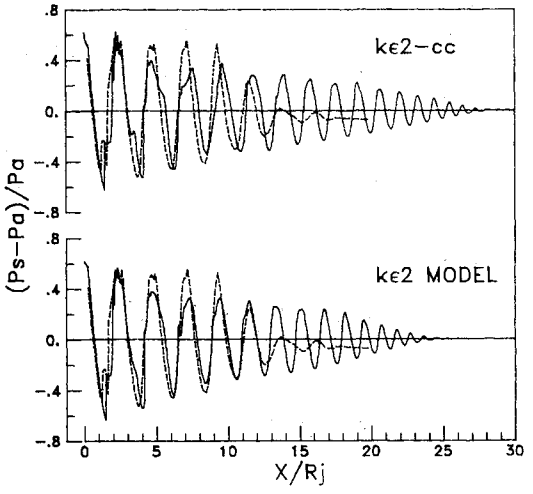

(a) CENTERLINE R/Rj = 0.0

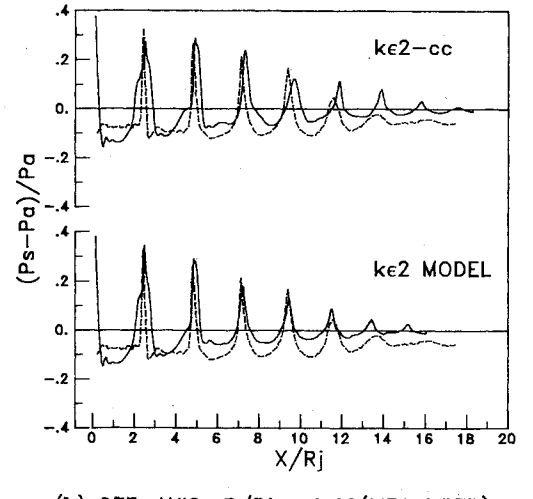

(b) OFF−AXIS R/Rj = 0.90(MEASURED)
0.75(PREDICTED)

Fig. 10 Effect of turbulence closure model on predicted plume static pressure for underexpanded $M_e = 1.0$, $P_e/P_a = 1.62$ flow;—— predicted $M_f = 0.15$; ----measured.

Prediction of the Broadband Shock Noise Spectrum Peak Value

Far-field acoustic spectra associated with shock-containing supersonic jet plumes exhibit characteristic spectral features that often clearly indicate the presence of shock noise. A representative example far-field ($R/R_j = 122$) narrowband acoustic spectrum is furnished in Fig. 11. Both the frequency f_p at the spectrum peak value and its second harmonic can be observed in this figure. The spectral data refer to acoustic radiation at 150 deg to the jet axis of the $M_e = 1.99$ supersonic nozzle for the overexpanded condition at $P_e/P_a = 0.421$.

Harper-Bourne and Fisher[3] have studied the nature of the broadband shock noise process associated with sonic nozzles (i.e., $M_e = 1.0$). They found that the shock noise frequency f_p varied inversely with an average shock cell spacing, and that this frequency was Doppler shifted after examining acoustic radiation at various angles to the jet axis. This Doppler shift was modeled by Harper-Bourne and Fisher in terms of a line array of monopole sources (located at the shock termination points) whose phasing is governed by the travel time of the relevant convected turbulence. Their model suggested that shock noise would exhibit a peak value at a frequency given by

$$f_p = U_c/L(1 - M_c\cos\theta) \tag{1}$$

where $M_c = U_c/C_0$, U_c is the convection velocity of the related turbulent disturbances, C_0 the ambient sound speed, θ the angle to the jet axis, and L an average shock cell spacing of the sonic nozzle's plume shock structure. In their work the average shock cell spacing was defined for a given nozzle pressure ratio to be the distance between the first and eighth shock average by the number of shocks over this distance. Harper-Bourne and Fisher obtained good agreement between the relative variation of their measured frequency data and that predicted by the Doppler shift in Eq. (1). However, careful examination of their frequency data has shown that Eq. (1) poorly agrees with their measured frequency values when using their average shock cell spacing. The data of Seiner and Norum[4-6] have also shown that Eq. (1), with a similarly defined average shock cell spacing, poorly predicts the measured f_p for both sonic and supersonic exit Mach number nozzles.

Before going further, it is necessary to examine the nature of the discrepancy between measured and computed values of f_p. As is shown by the plume static pressure comparisons in a previous section of this paper, the shock cell spacing diminishes with increasing distance from the nozzle exit. The Harper-Bourne and Fisher model requires at least two to three shock cells with a turbulence coherence over this distance to numerically describe far-field acoustic behavior. Without knowing any detailed preference for which shocks are likely to dominate the shock noise process leads one to consider an average shock cell spacing as the candidate aerodynamic length scale. However, recent measurements[6,7] attempting to determine the existence of any preferred region for broadband shock noise production show that the major component originates from near the end of a plume's potential core. The reported results refer to observed behavior associated with the sonic nozzle at $P_e/P_a = 1.90$, and the supersonic $M_e = 1.41$ nozzle at $P_e/P_a = 1.79$. These results suggest that the characteristic aerodynamic length scale for the shock-associated noise would be represented better by the shock cell spacing at the end of the plume's potential core. We now examine the consequence of such a choice for L in Eq. (1) by first making comparisons to measured data, and then proceed to show how well the numerically simulated jet plume (SCIPVIS) can be used to predict f_p.

At normal viewing angles to the jet axis in the acoustic far field Eq. (1) can be written as

$$L_e/\lambda_p = M_c \qquad (\theta = 90 \text{ deg}) \tag{2}$$

where L_e denotes the shock cell length at the end of a plume's potential core, λ_p the acoustic wavelength at the spectrum peak value, and M_c the Mach number at which disturbances

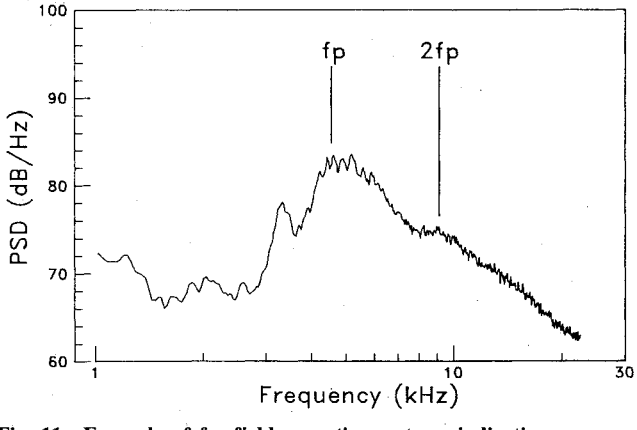

Fig. 11 Example of far-field acoustic spectrum indicating presence of shock noise.

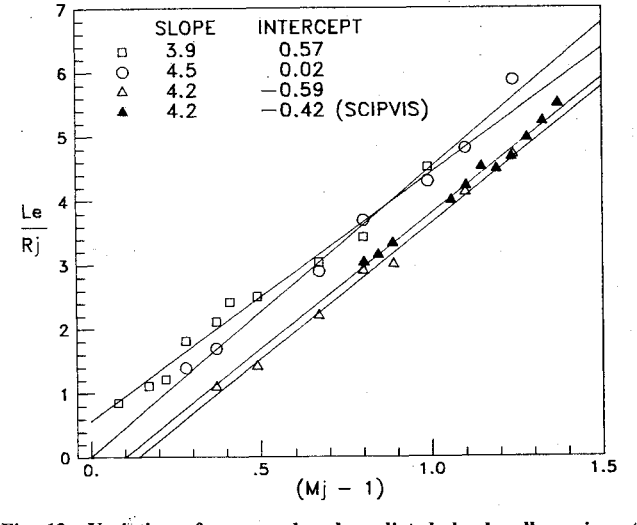

Fig. 12 Variation of measured and predicted shock cell spacing at end of potential core with fully expanded Mach number.

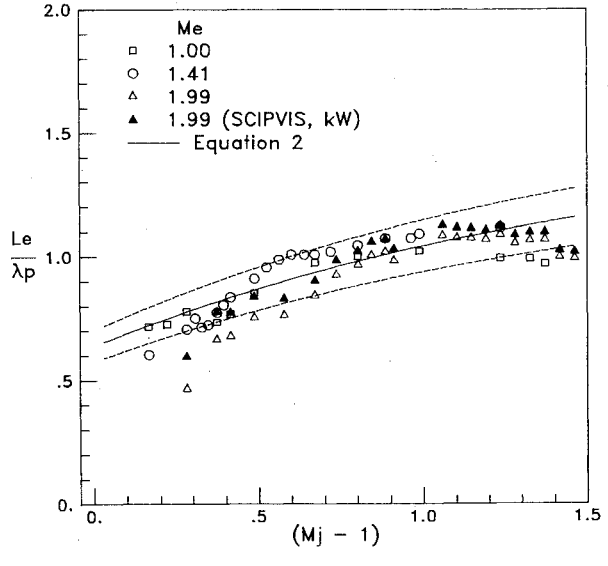

Fig. 13 Variation of measured and predicted L_e/λ_p with fully expanded Mach number.

are convected through the shock structure. Equation (2) represents the starting point for which comparisons are to be made with measured values of f_p, and the value of L_e is taken to represent the shock spacing that characterizes the two to three shock cells needed in the Harper-Bourne and Fisher model.

The variation of measured L_e with the jet's fully expanded Mach number M_j is shown in Fig. 12 for all three nozzles examined in the previous section (i.e., $M_e = 1.00$, 1.41, and 1.99). The measured values for L_e are obtained from the static pressure data of the previous section using the empirical relationship of Nagamatsu and Horvay[10] relating plume core length to the fully expanded jet Mach number M_j. The fully expanded Mach number M_j can be obtained from the isentropic equation relating nozzle pressure ratio to Mach number. The results in Fig. 12 indicate that an essentially linear relationship can be established between L_e and M_j. The least-squares fit for each nozzle, whose coefficients are listed in Fig. 12, are now used with measured values of λ_p to examine the relevancy of Eq. (2), or, equivalently, the Harper-Bourne and Fisher model.

For purposes of this comparison relevant disturbances will be assumed to be convected through the shock structure near the end of the potential core at a constant percentage of the jet's fully expanded velocity U_j. Thus, for all three nozzle cases, it is assumed that $U_c = 0.7U_j$. The value of 0.7 represents typical results obtained by Harper-Bourne and Fisher[3] for the sonic nozzle using their dual-beam laser schlieren method to obtain convection velocities from in-flow coherence measurements. Norum and Seiner[6] also obtained a similar result for both the sonic and supersonic exit Mach number nozzles by examining Doppler shifted acoustic far-field spectra.

Figure 13 shows how the measured ratio L_e/λ_p varies as a function of M_j for the three nozzle cases. The solid line represents the prediction of this ratio using Eq. (2), whose values are obtained by computing an idealized M_c as discussed above. As can be observed, Eq. (2) describes the general trend of the data, the majority of data values falling within $\pm 10\%$ of the predicted value as indicated by the upper and lower dashed curves. This is entirely adequate for it is difficult to establish any greater accuracy than this for measured λ_p.

Closer examination of Fig. 13 shows that the largest deviations from the predicted value for L_e/λ_p occur when strong shocks are present in the plume. Strong shocks can be expected when a nozzle's exit static-to-ambient pressure ratio falls outside the range $0.5 \le P_e/P_a \le 2.0$. For the $M_e = 1.99$ nozzle strong shocks begin to form slightly within this range, and, in particular, at values of $(M_j - 1)$ less than 0.7 and greater than 1.3. As can be noted from Fig. 13, this is the range where largest deviations occur from the predicted value. Unpublished preliminary plume Mach number measurements at NASA Langley show that the value M_j is significantly less than that computed from the isentropic relations when strong shocks are present in a plume. Accounting for this would produce a lower estimate for M_c, and perhaps a better agreement to the data in Fig. 13.

The overall agreement obtained between measured L_e/λ_p and that predicted by Eq. (2) clearly indicates that the Harper-Bourne and Fisher model adequately describes essential features of the physical process for broadband shock noise. This result, however, can only be achieved by considering the shock cell spacing at the end of a plume's potential core as the relevant aerodynamic length scale, rather than the average shock cell length as described by Harper-Bourne and Fisher.[3] We now examine how well the simulated numerical plume (SCIPVIS) predicts the characteristic aerodynamic length scale and affords prediction of f_p at various angles to the jet axis where shock noise is predominant. Only the $M_e = 1.99$ nozzle case is considered at this time.

Predicted values for L_e/R_j are shown in Fig. 12 as the solid symbols, and as can be observed a good correspondence exists to measured values. The predicted values are obtained by using the kW turbulence closure option of SCIPVIS, and the extrapolated value for L_e/R_j at $M_j = 0$ as would, for example, be deduced from the results in Fig. 7. The solid symbols in Fig. 13 refer to data obtained using the best-fit line for predicted L_e/R_j of Fig. 12 and measured λ_p. In the overexpanded region of flow (i.e., $M_j < 1.99$) a slightly better comparison to the predicted values of Eq. (2) is obtained for the $M_e = 1.99$ nozzle. The influence of strong shocks in the highly over- and underexpanded regions is still apparent from this comparison as discussed previously.

Frequency data as shown in Fig. 13 are more customarily presented in terms of a Helmholtz number based on the nozzle exit diameter and ambient sound speed (i.e., $H = f_p D/C_0$). Figure 14 displays the variation of the measured Helmholtz number for the $M_e = 1.99$ nozzle with fully expanded Mach number for radiation at $\theta = 90$ deg. The solid line represents prediction of the Helmholtz number based on Eq. (2) using the SCIPVIS-predicted values for L_e/R_j. As can be observed, the prediction of the Helmholtz number using an idealized estimation for M_c and the SCIPVIS code's prediction of L_e/R_j provides satisfactory agreement over a wide range of nozzle pressure ratios where corresponding far-field acoustic data have been obtained. The variation of f_p in terms of the Helmholtz number to various angles to the jet axis is shown in Fig. 15. Equation (1) is used to predict this Helmholtz number using values obtained by SCIPVIS for L_e/R_j. The data in Fig. 15 include both an over- and underexpanded condition for the

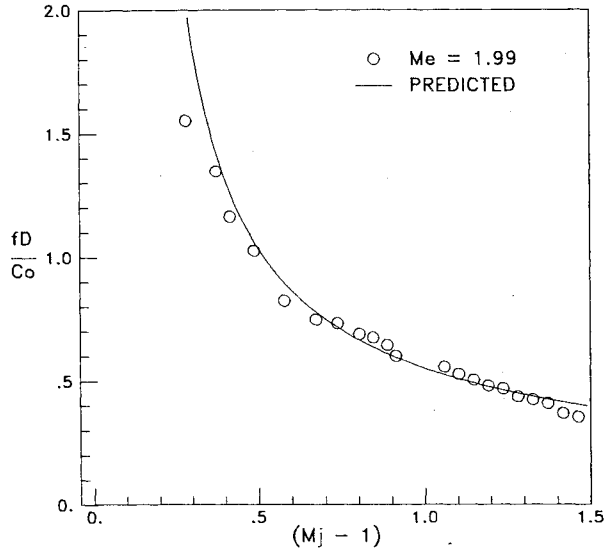

Fig. 14 Comparison of predicted and measured peak frequency for broadband shock noise at 90 deg to jet axis.

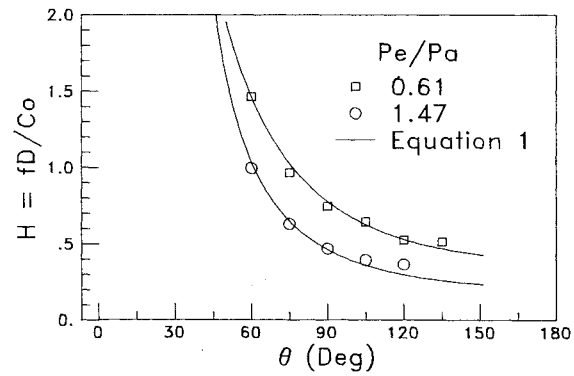

Fig. 15 Comparison of predicted and measured peak frequency for broadband shock noise at various angles to jet axis.

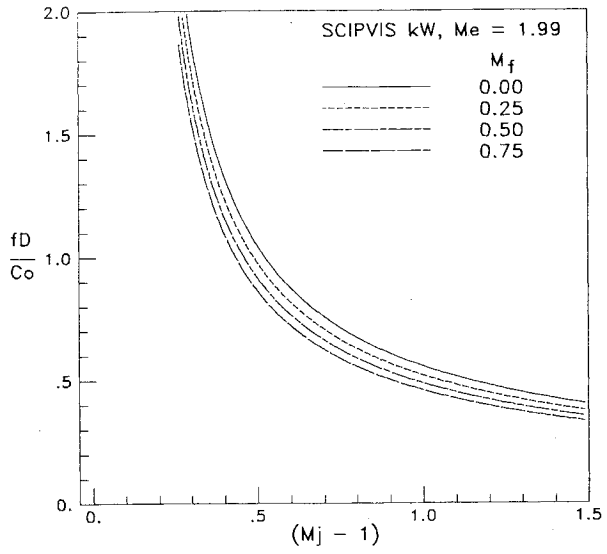

Fig. 16 Predicted effect of flight on peak frequency for broadband shock noise.

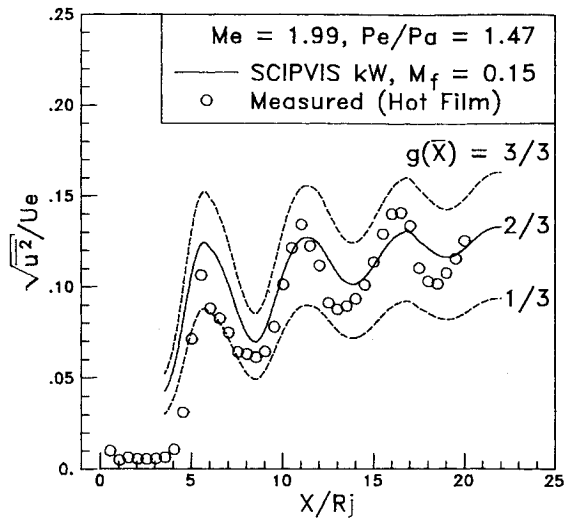

Fig. 17 Axial evolution of longitudinal turbulent component along jet lipline for an underexpanded supersonic jet.

$M_e = 1.99$ nozzle, and as can be seen a good agreement is obtained between prediction and measurement. Both Figs. 14 and 15 indicate that the Harper-Bourne and Fisher model is relevant to the observed physical process, that the shock cell spacing at the end of a plume's potential core L_e is the characteristic aerodynamic scale for the process, and that the numerically simulated jet (SCIPVIS) performs adequately to aid in prediction of f_p.

The advantage of using SCIPVIS to provide prediction of f_p lies in its ability to include practical conditions that are not as easily simulated in a model jet laboratory. Example conditions include the simulation of the total temperature of a full-scale engine plume, and forward flight speed effects for either subsonic or supersonic aircraft. At this time only the subsonic forward speed effects on f_p will be considered.

Using the flight Mach number effects on the shock cell spacing L_e as previously shown in Fig. 7, the SCIPVIS code can be used to provide an estimate for the modification to the broadband shock noise spectrum peak value f_p. This result is illustrated in Fig. 16, and covers the range of what might be expected for flight Mach numbers ranging from static to high subsonic $M_f = 0.75$. As is evident from this figure, the expected value for f_p decreases with increasing flight speed. Future experiments are currently being formulated to assess the validity of the forward flight predictions shown in Fig. 16.

The good agreement obtained for f_p using L_e does suggest that the major part of broadband shock noise is generated in the region near the end of the potential core. In this region the turbulence level in the mixing layer achieves maximum intensity,[11] and hot-film near-field microphone correlations[7] bandpassed around f_p reach a maximum amplitude. To properly examine the possibility that the major part of broadband shock is generated from this vicinity of the flow requires computation of the noise amplitude associated with individual shock-turbulent interactions.[1,2] The classical shock-vortex interaction problem as modeled by Ribner,[12] Weeks and Dosanjh,[13] and more recently by Pao and Salas,[14] offers some insight into the problem. A realistic prediction of the radial variation of oblique shock strength and local turbulence structure is required. We now consider at what stage the SCIPVIS code is to provide these fundamental requirements.

Prediction of Oblique Shock Strength

The SCIPVIS numerical code uses shock-capturing methodology in its computational scheme, but does not yet contain the necessary logic to properly identify wavefront locations. Suitable characteristic ray tracing techniques exist that should be able to meet the above requirement. To calculate the broadband shock noise energy radiated requires in addition (e.g., Ref. 2) estimation of the turbulent energy traversed by the shock.

Comparison of Measured and Computed Turbulence Intensity

In this section the measured longitudinal turbulence intensity is compared to that derived from the SCIPVIS code using the *kW* option. Again the trial case $M_e = 1.99$, $P_e/P_a = 1.47$ is used for purposes of comparison.

The experimental data were obtained using a wedge hot-film probe, whose behavioral response has been found to differ from that of hot wires in the transonic and supersonic flow regimes. A complete analysis of the probe's operational characteristics has been recently published in Ref. 15. However, since only one temperature overheat was used to acquire the data for this trial case, the approximate data-reduction procedure of Ref. 11 has been used to interpret the experimental data presented in this section.

As discussed previously the SCIPVIS code contains a transport equation for the turbulent kinetic energy k. As such we shall have to provide an estimate to obtain the longitudinal turbulence intensity component $(\overline{u'^2})^{1/2}/U$ from k. The turbulent kinetic energy per unit mass is defined as

$$k = \tfrac{1}{2}\overline{u_i u_i} = \tfrac{1}{2}[\overline{u'^2} + \overline{v'^2} + \overline{w'^2}] \tag{3}$$

From this relationship the longitudinal turbulence intensity can be written as

$$(\overline{u'^2})^{1/2}/U = (2g(\bar{x})k)^{1/2}U^{-1} \tag{4}$$

where the function $g(\bar{x})$ represents the fractional part of k due to longitudinal fluctuations. With shock-containing supersonic jet plumes virtually nothing is known about how this function varies in the shear layer. Its numerical value can, of course, never exceed 1, and probably never is less that $\frac{1}{3}$, which describes a state of isotropic turbulence. Actual values taken by the function $g(\bar{x})$ should fall between these limits.

Using the above estimate, Fig. 17 shows the agreement obtained along the jet lipline $r = R_j$ between the hot-film measurements (open symbols) and those estimated by the SCIPVIS code. The data are expressed in terms of the absolute turbulence exit intensity, where U_e represents the jet velocity. The upper and lower bounds are shown by the dashed lines, and it is evident that the measured data fall within this envelope. The solid line is obtained by assuming that $g(\bar{x})$

stays constant with a value of ⅔ along the lipline. It is known from Ref. 15 that these experimental data contain contributions from both density and temperature fluctuations, so that future measurements using the more exacting analysis of Ref. 15 should slightly lower the measured data presented in Fig. 17.

Both the measured and predicted turbulence data indicate that the turbulence level peaks at the end of a compression zone, and is a minimum at the end of an expansion zone. Differences between the measured and predicted axial locations for the minima and maxima originate from the SCIPVIS code's prediction for the location of oblique shock along the lipline.

The comparison in Fig. 17 is very encouraging. As can be observed, the general details of the variation of the predicted turbulence intensity level appear consistent with the measured variation. Coupled with a reasonable estimate for shock strength, the SCIPVIS code can eventually be expected to mediate theoretical prediction of radiated broadband shock noise energy.

Concluding Remarks

In this study the SCIPVIS plume model has been analyzed to determine its effectiveness to predict the complicated flow structure associated with supersonic shock-containing jet plumes. In particular this analysis has been conducted to assess the applicability of using this code as a key element in implementing a theoretical prediction scheme for shock noise radiation.

The analysis has been carried out for several exit Mach number cases (i.e., $M_e = 1.00$, 1.41, and 1.99) covering both under- and overexpanded flow conditions. All three turbulence closure models contained in the code have been used for comparisons to measured plume static pressure distributions. The principal findings of this study are as follows:

1) The prediction of plume static pressures for all three nozzle exit Mach numbers was found to agree exceptionally well with experimental data for both under- and overexpanded cases. The $k\epsilon 2$ turbulence closure model was found to uniformly underestimate shock locations, whereas the $k\epsilon 2$-cc model overestimated shock locations. The kW model provided the most uniform agreement with measurements for the supersonic nozzles.

2) The SCIPVIS code inadequately predicts resonant supersonic jets (i.e., those dominated by the screech mode).

3) The Harper-Bourne and Fisher phased-array model of shock noise correctly predicts the observed Doppler shift in terms of reception angle. For prediction of the spectral peak frequency f_p, a reinterpretation of the effective shock spacing is required: this must be taken as the value L_e at the end of the plume potential core in order to match experimental values. A rationale for this is given in the text.

4) Computations performed using the SCIPVIS code to compute L_e for the $M_e = 1.99$ nozzle provided an excellent match to measured L, and using an idealized value of M_c was found to adequately predict f_p for a wide range of nozzle exit static pressure ratios and angles to the jet axis. Increasing forward flight speeds, as predicted by SCIPVIS, produced a decreasing value for the estimated f_p.

5) The spatial variation of the turbulent kinetic energy was found to be in qualitative agreement with wedge hot-film turbulence measurements.

6) The SCIPVIS code requires coupling with a potential flow solver to incorporate the influence of jet entrainment effects on the external pressure field and streamwise velocity. These effects influence the far-field wave structures, but have little influence on the first several shock cells.

7) The SCIPVIS code requires an additional routine to provide for an appropriate estimate of the varying oblique shock strength in the mixing layer.

Overall the SCIPVIS code offers excellent potential for future incorporation into a program for shock noise estimation from supersonic flows containing either weak or strong shocks. Although not yet experimentally verified, it contains the necessary alogarithms to deal with high-speed, high-temperature jet plumes for aircraft in subsonic and supersonic flight (see Part I and Ref. 9). Future experimental efforts will be made in verifying the code's accuracy with respect to total temperature and forward flight effects. Both of these effects are expected to modify the broadband shock noise component due to alterations to the turbulent mixing process. Forward flight slows the rate of turbulent mixing, whereas heat addition lowers the plume density and enhances the turbulent mixing rate.

References

[1]Lighthill, M.J., "On the Energy Scattered from the Interaction of Turbulence with Sound or Shock Waves," *Proceedings of the Cambridge Philosophical Society,* Vol. 49, 1953, pp. 531-551.

[2]Ribner, H.S., "Acoustic Energy Flux from Shock-Turbulence Interaction," *Journal of Fluid Mechanics,* Vol. 35, Pt. 2, 1969, pp. 299-310.

[3]Harper-Bourne, M. and Fisher, M.F., "The Noise from Shock Waves in Supersonic Jets," AGARD-CP-131, 1973.

[4]Seiner, J.M. and Norum, T.D., "Experiments of Shock Associated Noise on Supersonic Jets," AIAA Paper 79-1526, 1979.

[5]Seiner, J.M. and Norum, T.D., "Aerodynamic Aspects of Shock Containing Jet Plumes," AIAA Paper 80-0965, 1980.

[6]Norum, T.D. and Seiner, J.M., "Broadband Shock Noise from Supersonic Jets," *AIAA Journal,* Vol. 20, Jan. 1982, pp. 68-73.

[7]Seiner, J.M. and Yu, J.C., "Acoustic Near Field and Local Flow Properties Associated with Broadband Shock Noise," AIAA Paper 81-1975, 1981.

[8]Pao, S.P. and Seiner, J.M., "A Theoretical and Experimental Investigation of Shock Associated Noise in Supersonic Jets," AIAA Paper 81-1973, 1981.

[9]Dash, S.M. and Wolf, D.E., "Interactive Phenomena in Supersonic Jet Mixing Problems," AIAA Paper 83-0288, 1983.

[10]Nagamatsu, H.T. and Horvay, G., "Supersonic Jet Noise," AIAA Paper 70-237, 1970.

[11]Seiner, J.M., McLaughlin, D.K., and Liu, C.H., "Supersonic Jet Noise Generated by Large Scale Instabilities," NASA TP-2072, 1982.

[12]Ribner, H.S., "The Sound Generated by Interaction of a Single Vortex with a Shock Wave," UTIA Rept. 61, 1959.

[13]Weeks, T.M. and Dosanjh, D.S., "Interaction of a Starting Vortex as well as a Vortex Street with a Travelling Shock Wave," *AIAA Journal,* Vol. 3, 1965, pp. 216-223.

[14]Pao, S.P. and Salas, M.D., "A Numerical Study of Two-Dimensional Shock Vortex Interaction," AIAA Paper 81-1205, 1981.

[15]Seiner, J.M., "The Wedge Hot-Film Anemometer in Supersonic Flow," NASA TP-2134, 1983.

[16]Dash, S.M., Wolf, D.E., and Seiner, J.M., "Analysis of Turbulent Underexpanded Jets, Part I: Parabolized Navier-Stokes Model, SCIPVIS," *AIAA Journal,* Vol. 23, April 1985, pp. 505-514.